Marine Geology 382 (2016) 151–161

Contents lists available at ScienceDirect

Marine Geology

journal homepage: www.elsevier.com/locate/margo

Sediment sorting and focusing in the eastern equatorial Pacific

Diksha Bista*,[1], Stephanie S. Kienast, Paul S. Hill, Markus Kienast

Department of Oceanography, Dalhousie University,1355 Oxford Street, PO Box 15000, Halifax, NS, B3H 4R2, Canada

ARTICLE INFO

Article history:
Received 28 August 2015
Received in revised form 21 September 2016
Accepted 26 September 2016
Available online 28 September 2016

Keywords:
Grain size
Sediment focusing
Sorting coefficient
Particle sorting
Eastern equatorial Pacific

ABSTRACT

The interpretation of sedimentary records in terms of glacial-interglacial changes in particle flux in the eastern equatorial Pacific (EEP) has been controversial. Here, we analyze disaggregated inorganic grain size (DIGS) distributions of three marine sediment cores from this region, focusing on the last 21 ka, to investigate evidence of sediment redistribution on the sea floor. Grain size sorting coefficients show that sediments in the EEP are moderately to well sorted, indicating sediment reworking in this region due to bottom currents. Furthermore, a systematic correlation between focusing factors and sorting coefficients at two sites shows that more focused sediments are also better sorted. We conclude that grain size based sedimentary records are consistent with the ^{230}Th-based evidence of lateral sediment redistribution on the sea floor in the EEP.

1. Introduction

The eastern equatorial Pacific (EEP) has been an area of interest for present and past biogeochemical studies because of its elevated primary productivity due to upwelling of nutrient rich subsurface waters. Considerable efforts have been made to reconstruct paleoproductivity in the EEP, the connection of this region to higher latitudes, and its link to climate variability on glacial-interglacial and millennial time scales (e.g., Calvo et al., 2011, Costa et al., 2016, Dubois et al., 2011, 2014, Hayes et al., 2011, Kienast et al., 2006, Lea et al., 2006, Loubere et al., 2004, Lyle et al., 2002, Patarroyo and Martínez, 2015, Pena et al., 2008, Pichat et al., 2004, Robinson et al., 2009, Winckler et al., 2016 and references therein). Several biological (Loubere, 2000) and geochemical proxies (Averty and Paytan, 2004) have been developed for reconstructing past changes in productivity and vertical flux. These proxies usually quantify changes in the burial flux of a biogenic component, which is then used to estimate vertical flux and paleoproductivity (Murray and Leinen, 1993; Murray et al., 2012; Paytan et al., 1996). However, the interpretation of sedimentary records in this region has been controversial.

Traditionally, the burial flux of a component is quantified as mass accumulation rate (MAR) based on linear sedimentation rate, dry bulk density and the concentration of the component of interest (DeMaster, 1981; Curry and Lohmann, 1986). The uncertainties associated with this method can be high, especially since it does not discriminate between vertical flux from the overlying water column (the variable of interest) and lateral flux from sediment redistribution on the sea floor due to bottom currents. The newer and increasingly used approach for estimating burial flux is based on the constant flux tracer ^{230}Th and is considered to provide more accurate estimates of vertical flux. Thorium-230 is produced uniformly in the water column by the decay of uranium-234 (^{234}U) at a known constant rate of 0.0267 dpm m^{-3} yr^{-1}. Thorium is highly insoluble in seawater and has a high affinity for particles, resulting in prompt removal from the water column as it adsorbs to settling particles (Bacon and Anderson, 1982; Francois et al., 2004; Henderson and Anderson, 2003). Based on the particle-reactive behavior of ^{230}Th, Bacon (1984) proposed that the flux of scavenged ^{230}Th to the sea floor is equivalent to its production from ^{234}U decay in the overlying water column. Therefore, the accumulation rate within a sediment horizon can be estimated by normalizing the known production rate of ^{230}Th to the concentration of ^{230}Th in the same horizon.

Export fluxes calculated using the traditional MAR and the ^{230}Th normalization method sometimes give divergent results, particularly in the equatorial Pacific (e.g., Anderson and Winckler, 2005; Averty and Paytan, 2004; Broecker, 2008; Francois et al., 2007; Kienast et al., 2007; Loubere et al., 2004; Lyle et al., 2005, 2007; Marcantonio et al., 2001; Paytan et al., 1996; Singh et al., 2011). Traditional MARs suggest large export fluxes (e.g., organic matter) and by inference higher primary productivity during the glacial period compared to the Holocene (Broecker, 2008; Lyle et al., 2002; Paytan et al., 1996). However, estimates based on ^{230}Th normalization show significantly

* Corresponding author.
E-mail addresses: dikshabista@gmail.com (D. Bista), stephanie.kienast@dal.ca (S. Kienast), paul.hill@dal.ca (P. Hill), markus.kienast@dal.ca (M. Kienast).
[1] Currently at School of Geographical Sciences, University of Bristol, Bristol, UK

http://dx.doi.org/10.1016/j.margeo.2016.09.016
0025-3227/

lower export flux (by 20–40 %) and little to no change in glacial and interglacial trends in the equatorial Pacific (Anderson et al., 2008; Higgins et al., 2002; Loubere et al., 2004; Marcantonio et al., 2001). The inconsistencies between these two methods have given rise to the "focusing debate" (Broecker, 2008; Francois et al., 2004, 2007; Lyle et al., 2005, 2007).

Studies supporting ^{230}Th normalization suggest that traditional MARs are influenced by lateral sediment redistribution that occurs in the deep Pacific Ocean, possibly in a systematic climate related fashion. Suman and Bacon (1989) quantified syndepositional sediment redistribution using the inventory of excess ^{230}Th in the sediment and introduced the "focusing factor". Calculation of the focusing factor (Ψ) is based on the assumption that the inventory of excess ^{230}Th in the sediment is equal to its production rate in the water column by uranium decay. If there is no syndepositional sediment redistribution on the sea floor, the ratio between inventory and production is equal to 1 ($\Psi = 1$). The inventory of excess ^{230}Th in the sediment will change if there is addition (focusing, $\Psi > 1$) or removal (winnowing, $\Psi < 1$) of sediment on the sea floor (Francois et al., 2004; Suman and Bacon, 1989). In the EEP, focusing factors as high as 10.5 have been observed (Singh et al., 2011) for glacial age sediments.

Studies challenging ^{230}Th normalization argue that sedimentary evidence does not support widespread sediment redistribution in the equatorial Pacific (Broecker, 2008; Lyle et al., 2005, 2007). These studies suggest that the observed high inventory of ^{230}Th in the sediment is due to boundary scavenging of dissolved ^{230}Th in the water column from areas of low particle flux, such as gyres, to areas of high particle flux, such as the equatorial upwelling region. Francois et al. (2007), however, argued that the low residence time of dissolved ^{230}Th ($<$ 4–40 yrs) and suspended particulates (5–10 yrs) inherently limits the lateral transport of both dissolved ^{230}Th and ^{230}Th attached to suspended particles. Hayes et al. (2013) found a uniform distribution of dissolved ^{230}Th despite spatial gradients in particle flux in the North Pacific Ocean. In the highly productive upwelling region off North West Africa, Hayes et al. (2015) constrained boundary scavenging of ^{230}Th to 40±10 % of its water column production. Siddall et al. (2008) used an ocean circulation model to further argue against the studies by Lyle et al. (2007) and Broecker (2008) and showed that boundary scavenging does not fully explain the high excess ^{230}Th accumulation observed in the Panama Basin. Similarly, Singh et al. (2013) found that the transport of dissolved ^{230}Th from the Peru Basin into the Panama Basin is relatively small and only contributes 15–30 % of the total dissolved ^{230}Th found within the water column of the Panama Basin itself. The lateral export of dissolved ^{230}Th between these two basins could only produce focusing factors of 1.3 and cannot explain the high focusing factors found at some sites in Panama Basin (Kienast et al., 2007; Singh et al., 2011).

In this study, we use disaggregated inorganic grain size (DIGS) measurements of EEP downcore sediments as an independent approach to investigate sea floor sediment dynamics over time. The DIGS distribution is a function of the physical processes affecting sediment transport and deposition, and records information about the environmental conditions under which the sediment was deposited (Folk and Ward, 1957; Kranck, 1975; Kranck and Milligan, 1985; Kranck et al., 1996a; Middleton, 1976). Grain size parameters such as mean size, sorting coefficient, and skewness are therefore used to gain insight into processes affecting the sediment prior to final deposition (Blott and Pye, 2001; Flemming, 2007; Folk and Ward, 1957). A particle with a given settling velocity (which is related to its grain size) gets deposited when the current shear stress is below its critical deposition stress. Sediment grains are hydrodynamically size sorted according to particle settling velocity and shear stress (Kranck and Milligan, 1985; McCave et al., 1995). During transport, particles with a larger settling velocity are deposited on the seabed while grains with smaller settling velocity are kept in suspension and

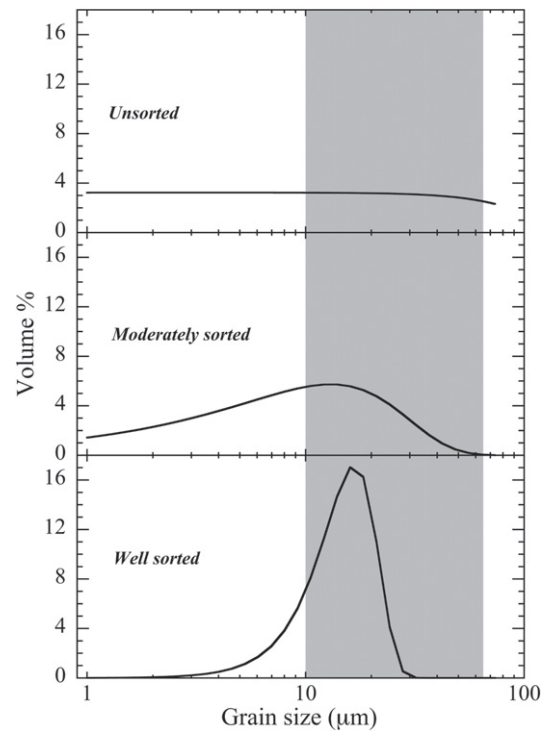

Fig. 1. Idealized DIGS distributions of an unsorted hemipelagic sediment, a moderately sorted, and a well sorted sediment on semi-log axes. The shaded area represents the sortable silt (10–63 μm) size range. The distribution of unsorted sediment (top panel) approximately follows the hemipelagic sediment observed by Rea and Hovan (1995). The distributions of moderately sorted (middle panel) and well sorted (bottom panel) sediment are similar to the size distribution of sediment from the Nova Scotian Rise at moderate and fast current velocity, respectively (McCave et al., 1995). Note that the well sorted sediment shows a narrower spread in its size distribution.

are transported further downstream (McCave et al., 1995; McCave and Hall, 2006). Thus, under the influence of bottom currents, an originally unsorted hemipelagic sediment becomes sorted according to settling velocity (grain size), and will display a mode in its DIGS distribution (Fig. 1). Sediments that have undergone multiple resuspension and settling events, therefore, display a narrow, well sorted DIGS distribution (McCave et al., 1995; McCave and Hall, 2006; Kranck et al., 1996a,b).

McCave et al. (1995) showed that in the deep sea, bottom current hydrodynamics mostly affect quartz grains in the sortable silt size range (10–63 μm) because of the tendency of material finer than 10 μm to behave cohesively, and because of the inability of average deep sea currents to move materials coarser than 63 μm (Ledbetter, 1986; McCave et al., 1995; McCave and Hall, 2006). Sediments in the sortable silt range are likely to be broken up and respond as single particles within the high shear region near the seabed. A high degree of sorting indicates that sediments have undergone lateral transport on the sea floor, so a positive correlation should exist between focusing factors and the degree of sediment sorting.

2. Methods

2.1. Core material and study area

Three cores from the EEP were studied for this project (Fig. 2, Table 1). ME0005A-27JC (hereafter referred to as ME-27) was recovered from 2203 m water depth on the southern side of the Carnegie Ridge, which forms the southern boundary of the Panama basin. Core TR163-19 (hereafter referred to as TR-19) was recovered

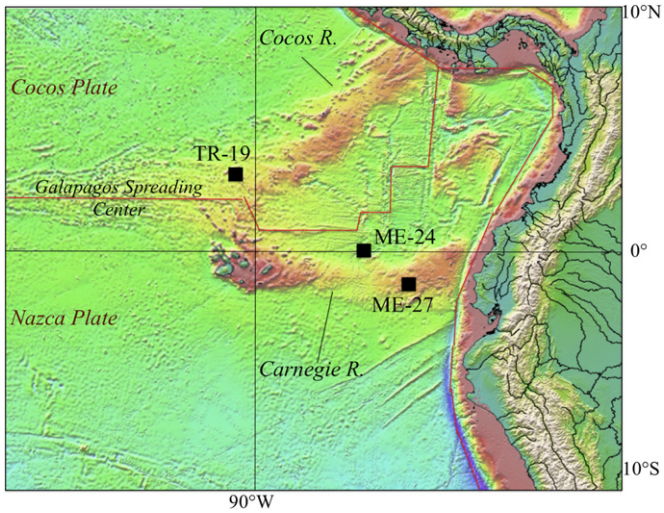

Fig. 2. Map of the core site showing cores TR163-19P, ME0005A-24JC and ME0005A-27JC. Bathymetry from Smith and Sandwell (1997) (http://topex.ucsd.edu/marine_topo/mar_topo.html)

from 2348 m water depth on the outer flank of the Cocos Ridge, which encloses the Panama basin in the northwest. Sediment core ME0005A-24JC (hereafter referred to as ME-24) was recovered from within the basin at the foot of the Carnegie Ridge at 2941 m water depth. Within the basin, the Cocos and Nazca plates are separated by the active Galapagos spreading zone that provides hydrothermal input to the surrounding area. Among the three EEP cores, ME-24 is affected most by hydrothermal input since this site is approximately 50 nautical miles south of the spreading center.

2.2. Core chronologies

The age models (Fig. 3) of all three EEP cores are adopted from Dubois et al. (2011) and references therein. The chronology for Marine Isotopic Stage 1 and 2 (MIS1 and MIS2) is based on 6 radiocarbon dates on *Neogloboquadrina dutertrei* for ME-24, 4 radiocarbon dates for ME-27, and on planktonic $\delta^{18}O$ stratigraphy augmented by 2 radiocarbon measurements for TR-19. Establishing absolute age control beyond MIS2 is notoriously difficult. In the case of the EEP, however, there are several high resolution records that are directly tied to northern and southern hemisphere forcing, which help constrain the age models. In particular, Dubois et al. (2011) discuss two viable age models for ME-24 beyond the oldest ^{14}C date of 20.79 ka at 351 cm. These scenarios are based on graphical correlation of millennial-scale events observed in opal and $\delta^{15}N$ records to the high resolution $\delta^{18}O_{ice}$ EPICA record in Antarctica. The resulting tie point during MIS3 between ME-24 and the EPICA record is at 38.9 ka BP (at 592.5 cm or 504 cm core depth respectively, in scenario 1 or 2). TR-19 and ME-27 were then graphically correlated to ME-24 using the AnalySeries software for the MIS3 time interval (for more details, see Dubois et al., 2011).

Table 1
Core locations and water depths.

Core ID	Latitude	Longitude	Water depth (m)
ME0005A-27JC	1° 51.201′ S	82° 47.20′ W	2203 m
TR163-19P	2° 15.5′ N	90° 57.1′ W	2348 m
ME0005A-24JC	0° 01.302′ N	86° 27.788′ W	2941 m

2.3. Focusing factor

The focusing factor estimates the extent of sediment redistribution on the sea floor using the inventory of $^{230}Th_{xs,0}$ (i.e. scavenged ^{230}Th corrected for decay) in the sediment. If the production rate (β_{230}) of ^{230}Th in the overlying water column corresponds to the flux of scavenged ^{230}Th to the sea floor, then the inventory of scavenged ^{230}Th in the sediment between core depth Z_1 and Z_2 should be equal to its production rate in the overlying water column integrated over the time of accumulation of the depth interval (Francois et al., 2004):

$$\int_{Z_1}^{Z_2} {}^{230}Th_{xs,0} \times \rho\, dz = \int_{t_1}^{t_2} \beta_{230} \times z\, dt \quad (1)$$

In Eq. (1), ρ is the dry bulk density ($\rho = 1/(3.6 - 0.0279 \times \% CaCO_3)$, Snoeckx and Rea, 1994) and t_1 and t_2 are the ages corresponding to core depths Z_1 and Z_2, respectively. This relationship only holds true if there is no syndepositional redistribution of sediment. Sediment redistribution on the sea floor changes the ^{230}Th inventory in the sediment. Suman and Bacon (1989) quantified syndepositional sediment redistribution by means of the focusing factor (Ψ) where

$$\Psi = \int_{Z_1}^{Z_2} \frac{{}^{230}Th_{xs,0} \times \rho}{\beta_{230} \times z \quad (t_2 - t_1)}\, dz \quad (2)$$

A focusing factor of 1 ($\Psi = 1$) indicates that accumulation of ^{230}Th in the sediment is equal to production of ^{230}Th in the overlying water column. A focusing factor greater than 1 ($\Psi > 1$) indicates lateral addition of ^{230}Th to a given site due to lateral sediment movement, whereas a focusing factor less than 1 ($\Psi < 1$) indicates winnowing i.e., the removal of ^{230}Th due to lateral sediment movement.

2.4. Grain size analysis

Prior to grain size analysis, samples were chemically pretreated following the procedures outlined by Mortlock and Froelich (1989) and McCave et al. (1995) to remove all biogenic material from the sediment. Organic carbon and carbonate were removed from subsamples (~0.5 g) using 10% hydrogen peroxide (H_2O_2) and 10% hydrochloric acid (HCl), respectively. The samples were dried overnight and then treated with 40 ml of 2 M sodium carbonate

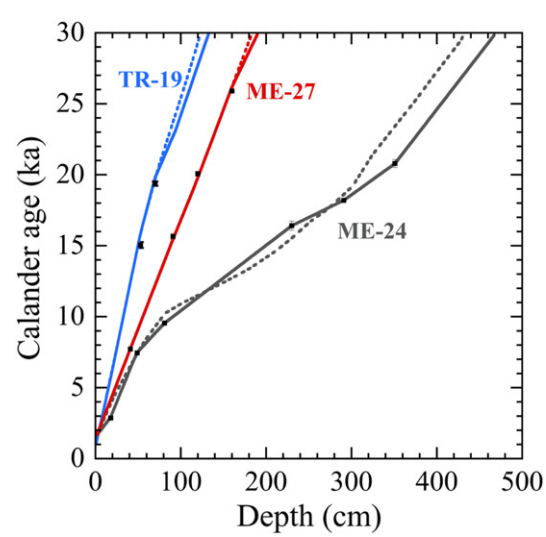

Fig. 3. Depth-age relationships for three EEP cores (solid lines) used in this study. Markers on solid lines represent radiocarbon dates with respective error bars. Dotted line shows the previously used chronology by Kienast et al. (2007).

(Na_2CO_3) solution in a hot bath (80 °C) for 5hrs to dissolve biogenic opal. This was followed by centrifugation and decantation of the Na_2CO_3 solution containing dissolved opal. The samples were rinsed three times with distilled water to remove all traces of Na_2CO_3.

Scanning electron microscope (SEM) images were taken to visually examine the sediment after the various pretreatment steps. Images were taken of bulk sediment, carbonate free sediment, and carbonate and opal free sediment of two marine standards (Std-1 and Std-2) that were created using sediments from the EEP. Prior to chemical treatment, the bulk sample contained diatoms, radiolarians, and carbonate shells (Fig. 4a). After treatment with H_2O_2 and HCl, no carbonate shells are seen in the images (Fig. 4b). After sequential opal removal, no diatoms or radiolaria are visible, and the SEM images only show inorganic grains (Fig. 4c). Collectively, these images indicate that the pretreatment procedures for removing organic matter, carbonate, and opal were successful.

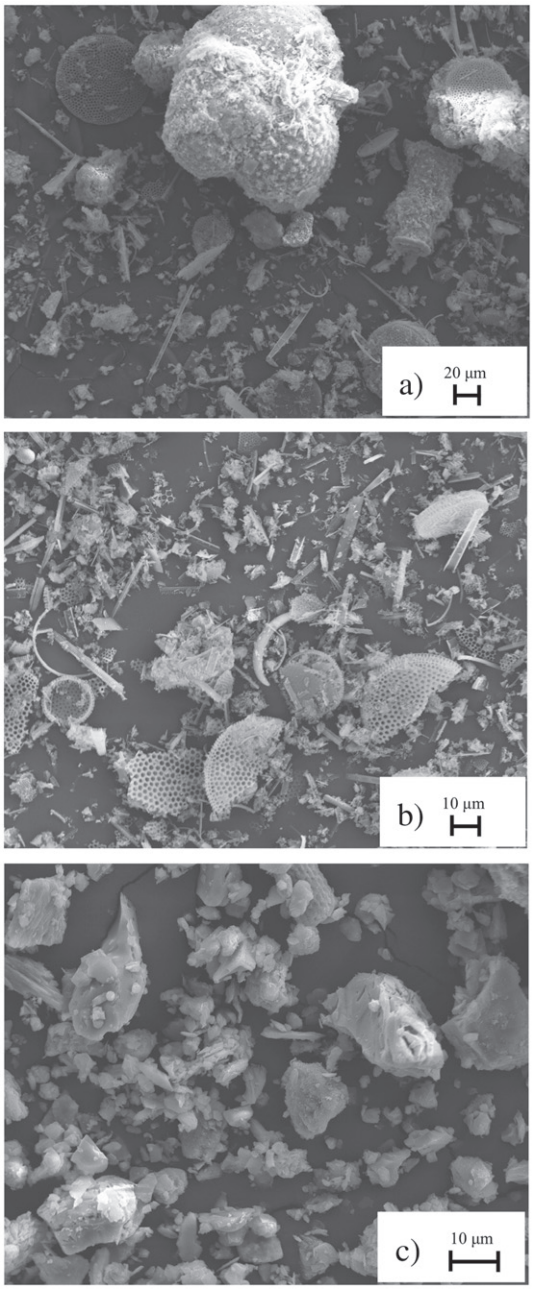

Fig. 4. SEM images of a (a) bulk sediment, (b) sediment from which organic carbon and carbonate have been removed and (c) inorganic sediment from which organic carbon, carbonate, and opal have been sequentially removed. Note different magnifications in each panel.

The residual inorganic sediment was then analyzed for its grain size distribution. DIGS distributions were obtained using a Beckman Coulter Counter Multisizer III following a procedure similar to the one described by Milligan and Kranck (1991). For this study, two aperture tubes (diameter 200 µm and 30 µm) were used to generate grain size distributions over the range of 1–100 µm. For more details on pretreatment and grain size analysis, see Bista (2015).

The analytical error of the Coulter Counter was determined by using a poorly sorted glacial sediment collected in Sillikers, New Brunswick, Canada. This standard is referred to as "Sillikers" and has a characteristic grain size distribution. Sillikers was run everyday the Coulter Counter was used to examine instrument error. The instrument as well as the pretreatment errors were estimated using the marine standards (Std-1 and Std-2). A subsample of both Std-1 and Std-2 was always treated along with the core samples to determine the reproducibility after the chemical pretreatment.

Twenty-three Sillikers replicates produced a mean distribution that has standard deviation in individual size bins ranging from 0.12 to 0.44 vol% (Fig. 5). Similarly, 13 replicates of each marine standard produced standard deviations in individual size bins ranging from 0.14 –0.48 vol% (Fig. 5). These deviations in each size bins are comparatively small given the volume distribution of the sediment samples.

2.5. Sorting coefficient

Sediment sorting occurs during resuspension and/or deposition. Sediment that has undergone hydrodynamic sorting shows a modal peak in its grain size distribution. The width of the peak depends on the degree of sorting (Fig. 1). If the sediment has undergone a high degree of sorting, the grain size distribution shows a narrow modal peak, conversely a less sorted sediment is expected to show a broader peak (McCave et al., 1995; McCave and Hall, 2006).

The degree of sorting can be calculated as the standard deviation (sorting coefficient) about the mean and reflects the variation in grain size classes that make up the bulk sediment. Since sorting of deep sea sediments largely occurs in the sortable silt size range (McCave et al., 1995; McCave and Hall, 2006), the sorting coefficient of the sortable silt fraction (10–63 µm) was calculated in this study. For this, the volume in each size class between 10 and 63 µm was first renormalized to 100%. The sorting coefficient (σ_g) of the sortable silt fraction was then calculated using the method of moments (Blott and Pye, 2001).

$$\sigma_g = \exp\sqrt{\frac{\sum_{m=10}^{63} f_m(\ln m - \ln \bar{x_g})^2}{100}} \tag{3}$$

where σ_g is the geometric standard deviation that represents the sorting coefficient, f_m is the renormalized volume fraction in size class m and $\bar{x_g}$ is the geometric mean of the distribution. The geometric mean is described quantitatively as

$$\bar{x_g} = exp\ \frac{\sum_{m=10}^{63} f_m \quad \ln m}{100} \tag{4}$$

A larger sorting coefficient indicates greater variation in grain sizes, i.e., a lower degree of sorting. Conversely, a smaller sorting coefficient indicates a higher degree of sorting. In the idealized distributions shown in Fig. 1, the sorting coefficient is 1.67 for the unsorted

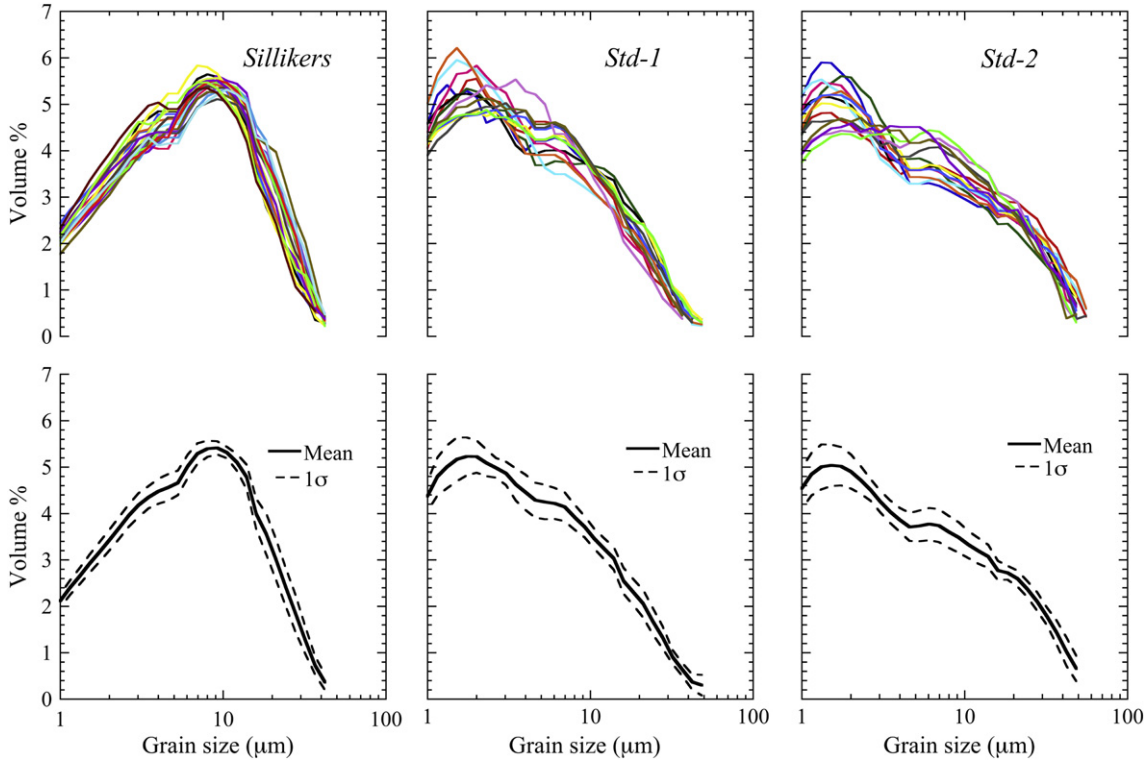

Fig. 5. Top panel: Replicate DIGS distributions of Sillikers (n = 23) and two marine standards, Std-1 and Std-2 (n = 13). Bottom panel: Mean DIGS distributions (solid black line) with 1σ (dashed black lines). The error of 0.48 vol % (upper limit of 1σ) in individual bins was considered to be the pretreatment and instrument error.

sediment (top panel), 1.48 for the moderately sorted sediment (middle panel) and 1.26 for the well sorted sediment (bottom panel). These values are calculated for the 10–63 μm size range. Sorting coefficients for the entire size distribution have different values but show the same trend among samples. The average sorting coefficients for Sillikers and marine standards (Std-1 and Std-2) replicates were found to be 1.42±0.02, 1.46±0.03, and 1.54±0.03, respectively. Therefore, measurement error for σ_g is estimated to be 0.03 units or 2%.

3. Results

The three EEP cores, in general, show bimodal DIGS distributions (Fig. 6). A dust mode is visible in the 1–5 μm size range (Prospero and Bonatti, 1969; Saukel et al., 2011), especially in TR-19 and ME-24, and another mode is seen in the sortable silt size range (10–63 μm). The position and the width of the sortable silt mode varies with the degree of sorting that has occurred in the sediment. In the representative DIGS distributions (Fig. 6), ME-27 shows coarser sortable silt modes and less sorting compared to the other two cores. The sortable silt mode in ME-24 is masked by the higher concentration of the dust fraction.

3.1. Sorting coefficients and focusing factors for the four time intervals

For consistency with previous studies (Kienast et al., 2007; Loubere et al., 2004), the focusing factors for the EEP cores were calculated using Eq. (2) for core top - 9.5, 9.5 –13.4, 13.4 –21, and 21–27 ka. Sorting coefficients were calculated using Eq. (3) for each sample that has a DIGS measurement and averages were provided for the time intervals mentioned above. Overall, sorting coefficients range from 1.36 –1.66, suggesting that these sediments are moderately to well sorted (Blott and Pye, 2001) (Figs. 7 and 8a). ME-27, which is at the shallowest water depth, is moderately well sorted and displays the smallest range in sorting coefficients (1.49 –1.58). In comparison, TR-19 is moderately well to well sorted (1.37 –1.56), whereas ME-24 ranges from moderately to well sorted (1.36 –1.66).

The EEP cores show focusing factors greater than 1 (Fig. 8b) implying lateral transport of sediments at these sites. There is an increase in focusing factors with increasing water depth. ME-27, recovered near the top of the Carnegie Ridge (2203 m wd), shows the lowest focusing factors and consistently is the least sorted. In contrast, ME-24 at the foot of the Carnegie Ridge (2941 m wd), shows the highest focusing during all time intervals and, at times, is also the best sorted (Figs. 8 and 9d).

Within each time interval, the correlation between focusing factor and sorting coefficient trends can be ambiguous (Fig. 8). For example, ME-24 shows highest focusing during the 13.4 –21 ka time interval whereas the average sorting coefficient does not show the most sorted sediment during this period. Based on elevated Fe/Al and Mg/Al ratios, ME-24 is likely affected by hydrothermal input in the 9.5 –13.4 ka time interval (Kienast et al., 2007), which would bias the grain size data. Hydrothermal activity can also lead to enhanced scavenging of ^{230}Th (Hayes et al., 2015), which would bias the focusing factor toward a higher value in this time interval. Lastly, some ambiguity could also arise because there is a high variability among sorting coefficients and the number of measurements is different in the different time intervals. Ignoring the 9.5 –13.4 ka time interval, which is affected by hydrothermal activity, and the single maximum sorting at 22 ka, sediments at site ME-24 are best sorted, on average, between 13.4 –21 ka, consistent with the highest focusing factor. Between 21–27 ka in ME-24, the focusing factor could be affected by the choice of age model (see Section 3.2). Similarly, based on the sorting coefficients, we would expect TR-19 to be more focused than ME-24 during the Holocene, which is not the case. Note, however, that there is no radiocarbon age during this time interval in TR-19 (Fig. 3).

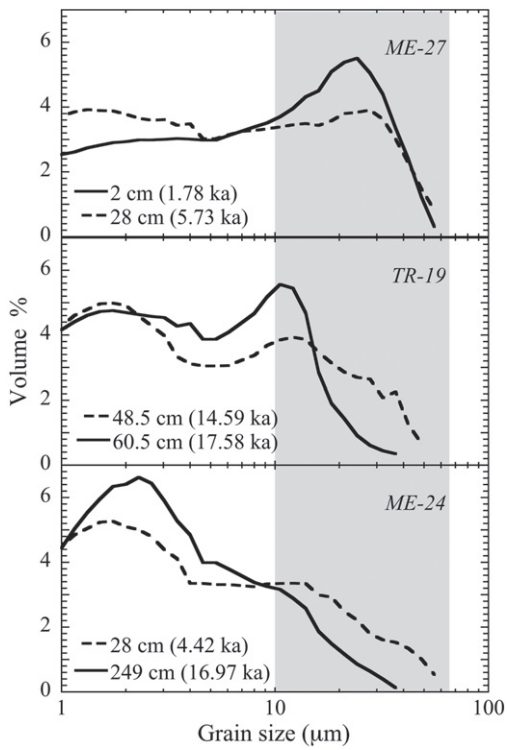

Fig. 6. Representative DIGS distributions for the three EEP cores with corresponding depth and age on semi-log axes. Distributions with lower sorting coefficients (more sorted) are represented by solid black lines and distributions with higher sorting coefficients (less sorted) are represented by dashed black lines. The shaded area represents the sortable silt size range (10–63 μm). The mode in 1–5 μm size range is dust (Prospero and Bonatti, 1969).

3.2. Sensitivity of focusing factors

In ME-24, the focusing factor was calculated based on two age model scenarios presented by Dubois et al. (2011). For the 21–27 ka time interval, the focusing factor changes from 4.8 (scenario 1 age model) to 3.2 (scenario 2 age model; included in Fig. 8b). In light of this sensitivity, and because there are no radiocarbon dates older than 21 ka in TR-19, we exclude data between 21–27 ka in all three cores to systematically evaluate the relationship between sorting coefficients and focusing factors. We also exclude data from the 9.5 –13.4 ka time interval in ME-24 for the correlation analysis due to the likely bias of the grain size data and ^{230}Th inventory by hydrothermal inputs (see above).

Focusing factors were also calculated between individual depths for which grain size data are available (Fig. 9). Note that this is not entirely justified, as core chronologies cannot be precisely constrained, and constant sedimentation rates between age control points have to be assumed. Nevertheless, given the exclusions described above, we think that presenting the data in this way and interpreting trends is valid.

3.3. Correlation between sorting coefficients and focusing factors

The Shapiro-Wilk test shows that both focusing factors and sorting coefficients are normally distributed in all three cores. Therefore, the correlation (r) between sorting coefficients and focusing factors was examined using a parametric Pearson's rho. Among the three cores, ME-27 does not show a correlation between sorting coefficients and focusing factors ($r = 0.43$ and $p = 0.12$, Fig. 9a). The lack of any systematic correlation might be because ME-27 has the smallest ranges and no significant trends either in focusing factors or in sorting coefficients (Fig. 8). There is a negative correlation between sorting coefficients and focusing factors in TR-19 ($r = -0.67$ and $p = 0.009$, Fig. 9b) and ME-24 ($r = -0.58$ and $p = 0.002$, Fig. 9c). The regression in ME-24 does not include the data between 9.5 – 13.4 ka. However, even when including the data during this time interval, ME-24 still shows a weak negative correlation between focusing factors and sorting coefficients ($r = -0.39$ and $p = 0.02$, not shown).

Fig. 9d shows the correlation between sorting coefficients and focusing factors for all EEP cores in one panel. The combined data clearly show that the site with the lowest focusing factors (ME-27) is also the least sorted. This is in contrast to the other two sites (ME-24 and TR-19), which are better sorted and have higher focusing factors. While both of these sites show relatively strong correlations between sorting coefficients and focusing factors, the absolute values from one site do not translate to the other site.

4. Discussion

4.1. Sources of sediment to the EEP

In the EEP, two major sources dominate the inorganic sediment within a few hundred kilometers of the continent; hemipelagic

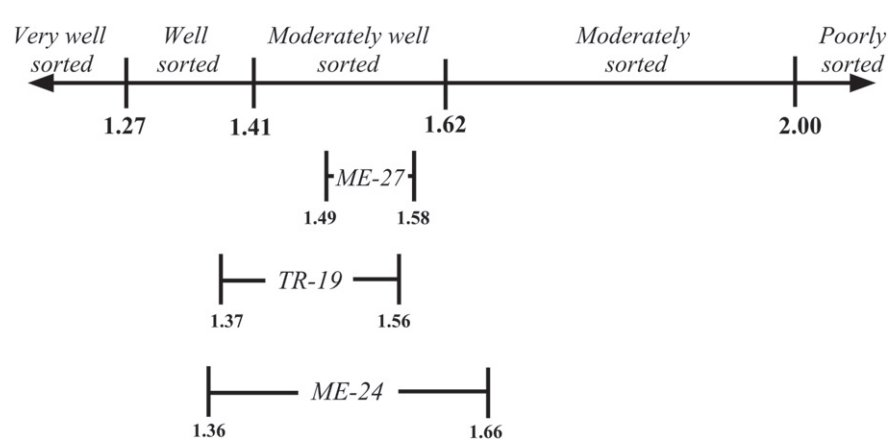

Fig. 7. Descriptive grade of sorting (Blott and Pye, 2001) and sorting coefficients calculated for the EEP cores using geometric method of moments (Eq. (3)).

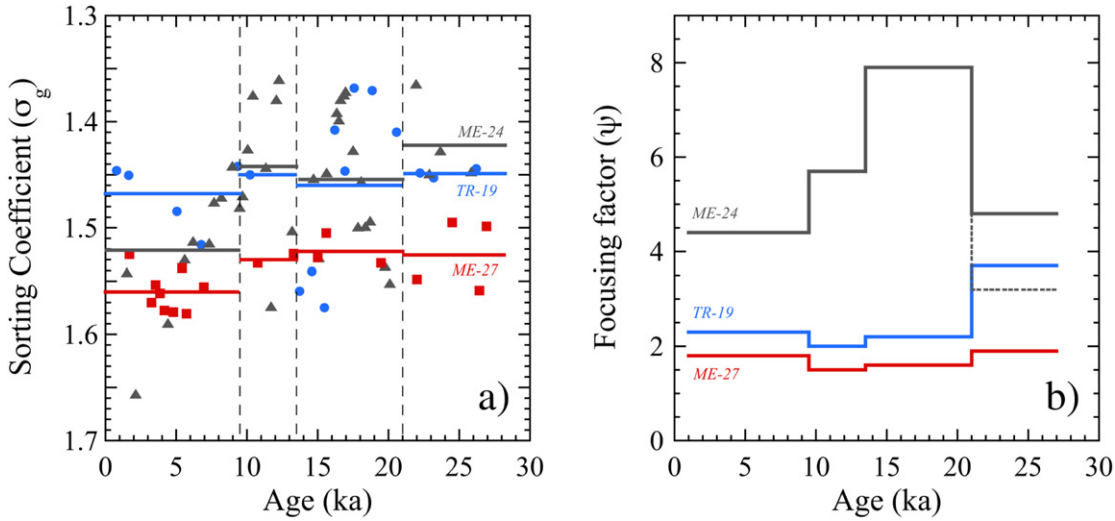

Fig. 8. a) Sorting coefficients calculated using Eq. (3) with reversed y-axis. A smaller sorting coefficient indicates higher degree of sorting. Vertical dashed lines represent the boundary between different time intervals and horizontal lines give the sorting coefficients averaged over the individual time intervals. Sorting coefficients for TR-19, ME-24, and ME-27 are represented by blue dots, gray triangles, red boxes, respectively. b) Focusing factors calculated using Eq. (2) for the three EEP cores. The time intervals are core top - 9.5, 9.5–13.4, 13.4– 21, and 21–27 ka. Dashed gray line shows the focusing factor calculated using the Scenario 2 age model presented by Dubois et al. (2011).

and eolian. The average percentages of inorganic material (100 - %$CaCO_3$ - %opal - %organic; data from Dubois et al. (2011), Kienast et al. (2007)) decrease offshore and are 34.4%, 27.5%, and 14.5% at sites ME-27, ME-24 and TR-19, respectively. We assume here that the inorganic sediment in the 10–63 μm size range is largely hemipelagic in origin. Rea and Hovan (1995) found that hemipelagic sediment shows a uniform grain size distribution with significant material coarser than 10 μm. Similarly, Boven and Rea (1998) found that material coarser than 10 μm in the EEP is dominantly hemipelagic and largely unsorted.

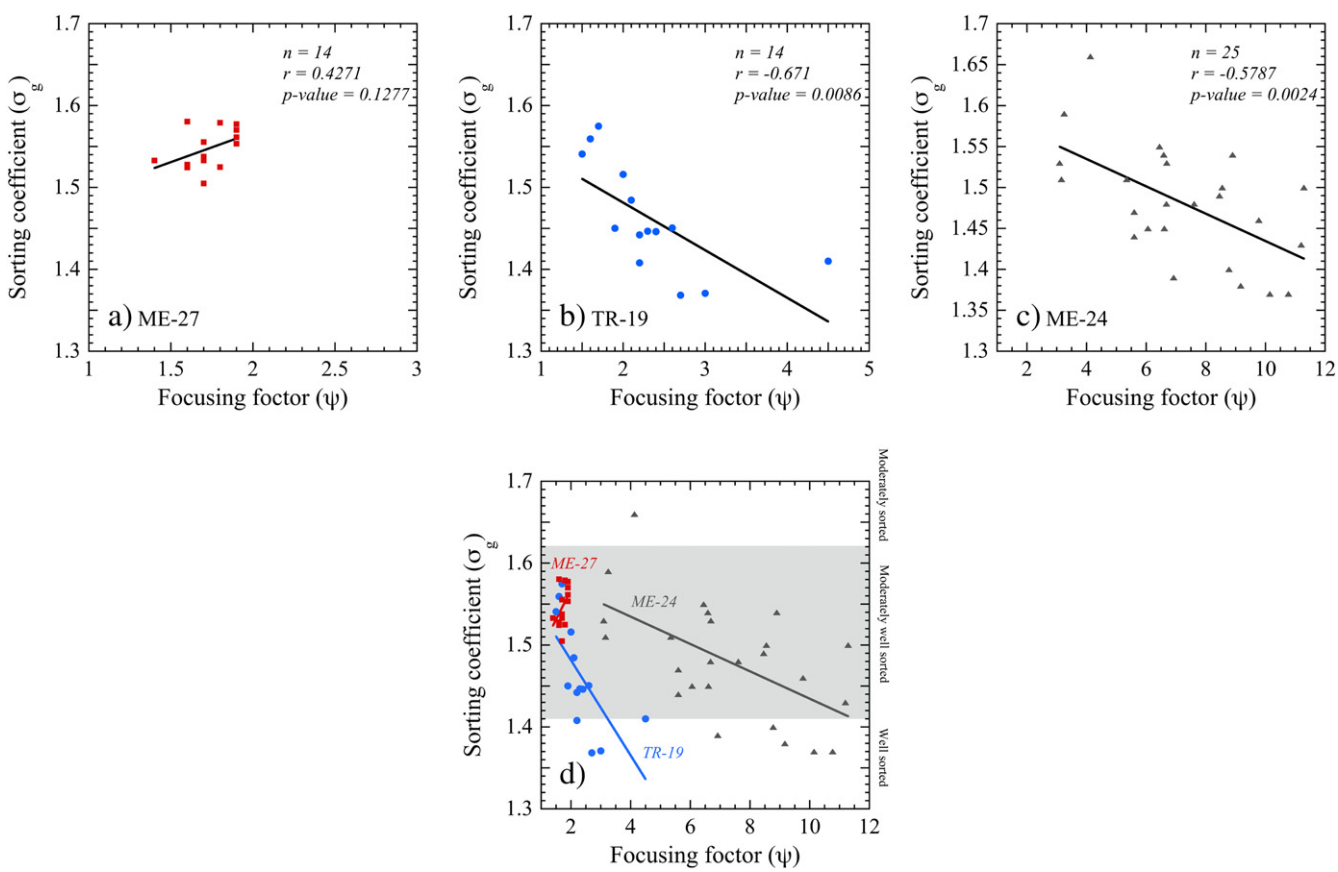

Fig. 9. Top panel: Correlation between sorting coefficients and focusing factors in individual EEP cores. The correlation coefficients (r) were calculated using the parametric Pearson's rho. A p-value <0.05 indicates that the data are correlated with each other. The regressions do not include data prior to 21 ka for all three cores (see text for details). ME-24 also excludes the depth interval influenced by hydrothermal input (9.5–13.5 ka, Kienast et al., 2007). Bottom panel: Correlation between focusing factors and sorting coefficients for all three EEP cores.

Eolian dust, which is size sorted during atmospheric transport, can be >10 μm when deposited close to its source area, and could thus bias our sorting estimates. However, Saukel et al. (2011) investigated the grain size composition of surface sediments from the tropical southeast Pacific and found that dust delivered to this region is fine (4–8 μm), consistent with direct observations by Prospero and Bonatti (1969). Saukel et al. (2011) also studied the clay mineralogy of surface sediments to identify the sediment populations that contribute to the inorganic fraction in the region. Based on the illite content of clay minerals, the authors find that dust from the Atacama desert is transported into the Panama Basin and as far north as 5°N. South American dust sources are consistent with lead isotope data from core sites in the EEP (Pichat et al., 2014) and the central equatorial Pacific (Reimi and Marcantonio, 2016). Both modeling and observational data show that most atmospheric aerosols are smaller than 10 μm (Mahowald et al., 2014). The DIGS distributions presented here show a pronounced modal peak in the <5 μm size range (Fig. 6) consistent with an eolian origin. Dust deposited in the EEP, therefore, does not influence the sorting coefficients calculated for the 10–63 μm size range, which is dominantly hemipelagic in origin.

Hydrothermal input from the Galapagos spreading center and other volcanic materials are also minor sediment sources to the EEP (Kienast et al., 2007; Saukel et al., 2011) and could potentially bias our results. However, we consider hydrothermal and volcanic inputs to be minimal except for the 9.5 –13.4 ka time interval in ME-24 where Fe/Al and Mg/Al show significantly elevated values (Kienast et al., 2007).

4.2. Focusing of the fine sediment fraction

Focusing factors of all EEP cores are greater than 1, indicating lateral sediment transport on the sea floor (Fig. 8b). Sorting coefficients show that sediments in the EEP are moderately to well sorted and indicate sorting by bottom currents (Fig. 8a). Bottom current induced sediment sorting is consistent with previous seismic and sedimentary studies that show heavily reworked sediments in the Panama Basin (Dubois and Mitchell, 2012; Heath et al., 1974; Lonsdale and Malfait, 1974; Malfait and Andel, 1980; Van Andel, 1973) and with a recent study at site ME-24 that infers current movement based on benthic foraminiferal analysis (Patarroyo and Martínez, 2015). Furthermore, the negative correlation between focusing factors and sorting coefficients (Fig. 9) shows that more focused sediments are also better sorted. Taken together, these results support the notion that lateral sediment redistribution affects sedimentation in the EEP.

The mean size of the sortable silt fraction and sorting coefficients follow the same trend (Fig. 10) indicating that sediments that are more sorted (lower sorting coefficient) have a lower mean grain size. Since sorting coefficients and focusing factors are negatively correlated, it also means that more focused sediments have a lower mean grain size. A decrease in the mean size together with an increased focusing factor can occur by addition of finer sediment to the site. At sites of faster bottom currents, finer sediments are winnowed out during size selective deposition and are transported further downstream (McCave and Hall, 2006). Deposition of winnowed fine sediment must occur somewhere downcurrent where the flow speed decreases. As a result, the winnowed sites would have an overall coarser mean size whereas sites downcurrent would consist of sediments with a finer mean size. In the EEP region, few studies on bottom current speed have been conducted (Gardner et al., 1984; Honjo et al., 1992; Johnson and Johnson, 1970; Lonsdale and Malfait, 1974; Lyle et al., 2014; Marcantonio et al., 2001). The average current velocity in the northern part of the Panama Basin, away from the stronger current that enters the Panama Basin along the Ecuador trench (Lonsdale and Malfait, 1974), is 5–7 cm s^{-1} (Gardner et al., 1984; Honjo et al., 1992). Further west at MANOP site C (~138° W), current velocities occasionally reach up to ~20 cm s^{-1}, but in general, predominant diurnal and semidiurnal currents are ~5 cm s^{-1} at the most (Lyle et al., 2014). The reported velocities in the EEP are thus slow enough for size selective deposition (<10–15 cm s^{-1}, McCave and Hall, 2006). Therefore, given the relationships between focusing factors, mean grain size, and sorting coefficients observed here, we conclude that fine sortable silts were dominantly transported to the core sites (sediment focusing), lowering the mean size of the sediment and, in the process, increasing the degree of sorting (lower sorting coefficient).

4.3. Influence of particle sorting on focusing factors

An important question is whether focusing factors are affected by the "particle sorting effect". Clay sized grains (<4 μm) have a high surface area and therefore adsorb more ^{230}Th (Francois et al., 2004; Kretschmer et al., 2010, 2011; McGee et al., 2010; Thomson et al., 1993). The elevated concentration of ^{230}Th in the fine fraction can lead to an overestimation of focusing factors and underestimation of vertical flux in areas of sediment focusing. Therefore, sediments that have undergone a higher degree of sorting could also, in principle, have an increased particle sorting effect on focusing factor estimates.

Kretschmer et al. (2010) found that 50–90 % of the total excess ^{230}Th inventory is concentrated in the<10 μm fraction, which leads to an overestimation of focusing factors up to 30% (carbonaceous) and 45% (siliceous sediment). If indeed 50–90 % of the bulk ^{230}Th were associated with the<10 μm fraction of the EEP sediments, there should be a positive relationship between ^{230}Th concentration and % fine fraction in a given sediment core. However, there is no such correlation in cores TR-19 and ME-24, and ME-27 shows the

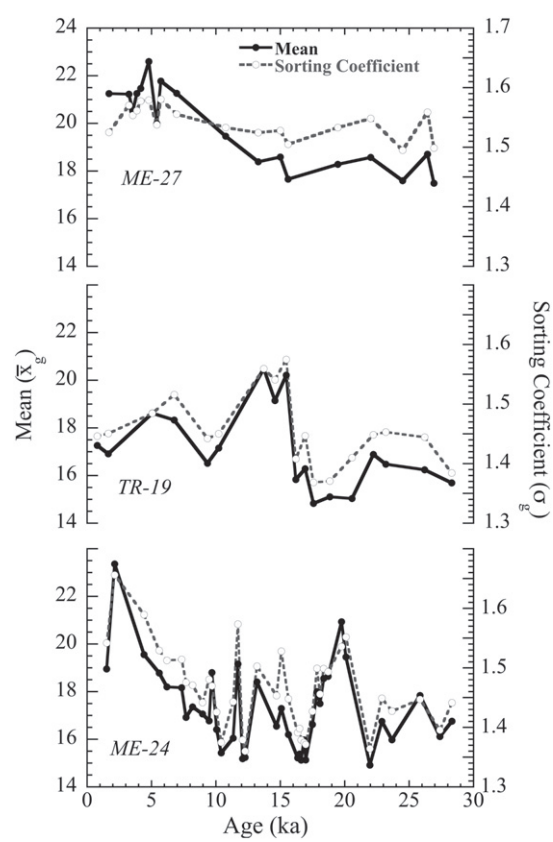

Fig. 10. Sorting coefficient (σ_g) and geometric mean ($\bar{x}_g$ in μm) calculated using Eq. (3) and Eq. (4), respectively for the EEP cores.

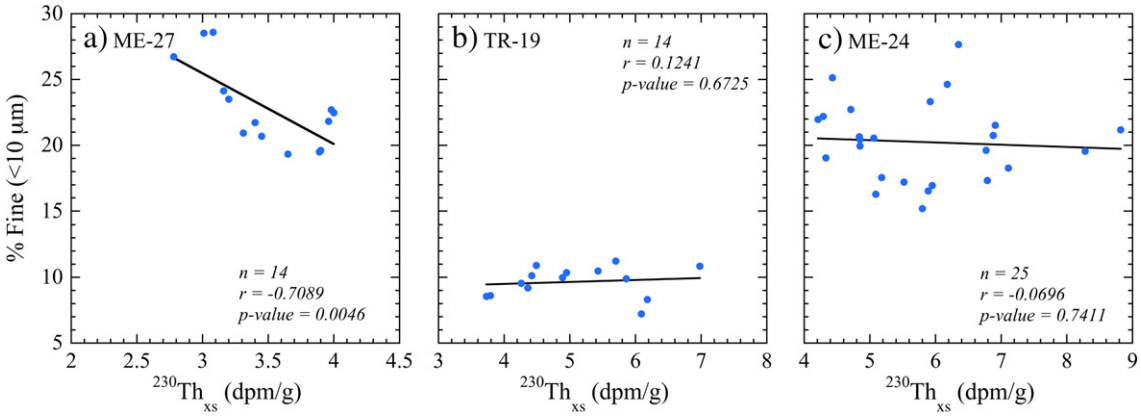

Fig. 11. Correlation between % fine fraction (<10 μm) and ^{230}Th concentration in bulk sediment. The data do not contain the 21–27 ka interval (see text for details). ME-24 also excludes the depth interval influenced by hydrothermal input (9.5–13.5 ka, Kienast et al., 2007). Correlation coefficients (r) were calculated using the parametric Pearson's rho. A p-value >0.05 indicates that the data are not correlated with each other (TR-19 and ME-24). In ME-27, the correlation is opposite to what is expected based on the grain size effect (see text for details).

opposite trend (Fig. 11), suggesting that the "particle sorting effect" in the EEP is small. Measurements of ^{230}Th in different size fractions are required to further confirm this result.

Kretschmer et al. (2010) conclude that ^{230}Th normalization is still a considerable improvement for vertical flux estimates compared to the traditional MAR approach, even with the grain size bias. Another study conducted on the Blake Ridge, a drift deposit in the western North Atlantic, showed only a minimal grain size bias on the bulk ^{230}Th inventory, despite the enrichment of ^{230}Th in the fine fraction (<4 μm) (McGee et al., 2010). This is likely due to the cohesive behavior of fine grains in marine settings, which limits the fractionation of grains <10 μm (McCave et al., 1995) or even <16 μm (Law et al., 2008) during lateral transport. Furthermore, Marcantonio et al. (2014) examined the inventories of ^{230}Th from winnowed and focused sites on the Cocos and Carnegie Ridges and speculated that the particle sorting effect occurs mostly at lower current velocities (3 cm s^{-1}) by preferential movement of the fine ^{230}Th rich fraction (detrital material, opal and organic carbon) which leaves the coarser fraction (foraminiferal carbonate shells) behind. The authors conclude that ^{230}Th normalization works well for recording fine grained fluxes, but is more problematic for coarse grained sediment fluxes in regions that have undergone sediment redistribution.

5. Conclusions

Downcore DIGS distributions in three EEP cores were analyzed in this study to examine the sediments for evidence of lateral transport along the sea floor over the last 21 ka. The sediments are moderately to well sorted, indicating bottom-current induced size sorting. In two of three cores (ME-24 and TR-19), we find a statistically significant negative correlation between focusing factors and sorting coefficients, showing more focused sediments are also better sorted. The third and the shallowest core (ME-27), which is at the top of the Carnegie Ridge, has the lowest overall focusing factors and also shows the least sorting among the three cores. Regionally, a simple relationship between sorting coefficients and focusing factors is not observed, possibly reflecting differences in the "upstream" properties of sediments delivered to the different sites and differences in local current regimes. Nevertheless, our study provides further evidence that the higher accumulation of ^{230}Th is chiefly controlled by syndepositional lateral sediment transport in the EEP (Francois et al., 2004, 2007; Kienast et al., 2007; Kusch et al., 2010; Loubere et al., 2004; Marcantonio et al., 2001; Siddall et al., 2008), rather than by a higher scavenging efficiency in the equatorial Pacific (Broecker, 2008; Lyle et al., 2005, 2007; Singh et al., 2011). Furthermore, in light of the study by Kretschmer et al. (2010), our results suggest that the grain size bias on bulk ^{230}Th concentrations in the EEP is small. Consequently, significant overestimation of focusing factors due to the particle sorting effect is unlikely.

Acknowledgments

We gratefully acknowledge the official reviewers of this manuscript for their helpful suggestions. Core material was kindly provided by the Core Repositories of Oregon State University (supported by NSF grant OCE97-12024) and the University of Rhode Island (supported by NSF grant OCE-9102410). We thank Jessica Carriere Garwood and Laura deGelleke for assistance with the grain size analysis. This research was supported by Natural Sciences and Engineering Research Council (NSERC grant 418518) Canada. We also acknowledge the support of the Canada Foundation for Innovation, the Atlantic Innovation Fund, and other partners which fund the Facilities for Materials Characterization, managed by the Institute for Research in Materials at which SEM images for this study were taken.

Appendix A. Supplementary data

Supplementary information and raw data associated with this article will be provided in an additional document. Supplementary data to this article can be found online at http://dx.doi.org/10.1016/j.margeo.2016.09.016.

References

Anderson, R.F., Fleisher, M., Lao, Y., Winckler, G., 2008. Modern $CaCO_3$ preservation in equatorial Pacific sediments in the context of late-Pleistocene glacial cycles. Mar. Chem. 111 (1), 30–46.

Anderson, R.F., Winckler, G., 2005. Problems with paleoproductivity proxies. Paleoceanography 20 (3), 381–398.

Averty, K., Paytan, A., 2004. A comparison of multiple proxies for export production in the Equatorial Pacific. Paleoceanography 19,

Bacon, M.P., 1984. Glacial to interglacial changes in carbonate and clay sedimentation in the Atlantic Ocean estimated from ^{230}Th measurements. Chem. Geol. 46 (2), 97–111.

Bacon, M.P., Anderson, R.F., 1982. Distribution of thorium isotopes between dissolved and particulate forms in the deep sea. J. Geophys. Res. 87 (C3), 2045–2056.

Bista, D., 2015. Reconstructing Dust Fluxes and Sediment Focusing in the Equatorial Pacific Over Glacial and Interglacial Time-Scales Using Grain Size Analysis. . Dalhousie University., Master's thesis June.

Blott, S.J., Pye, K., 2001. GRADISTAT: a grain size distribution and statistics package for the analysis of unconsolidated sediments. Earth Surf. Process. Landf. 26 (11), 1237–1248.

Boven, K.L., Rea, D.K., 1998. Partitioning of eolian and hemipelagic sediment in eastern Equatorial Pacific core TR 163-31B and the late Quaternary paleoclimate of the Northern Andes. J. Sediment. Res. 68 (5), 850–855.

Broecker, W., 2008. Excess sediment ^{230}Th: transport along the sea floor or enhanced water column scavenging? Global Biogeochem. Cycles 22 (1).

Calvo, E., Pelejero, C., Pena, L.D., Cacho, I., Logan, G.A., 2011. Eastern Equatorial Pacific productivity and related-CO_2 changes since the last glacial period. Proc. Natl. Acad. Sci. 108 (14), 5537–5541.

Costa, K., McManus, J., Anderson, R., Ren, H., Sigman, D., Winckler, G., Fleisher, M., Marcantonio, F., Ravelo, A., 2016. No iron fertilization in the equatorial Pacific Ocean during the last ice age. Nature 529 (7587), 519–522.

Curry, W., Lohmann, G., 1986. Late Quaternary carbonate sedimentation at the Sierra Leone Rise (Eastern Equatorial Atlantic Ocean). Mar. Geol. 70 (3-4), 223–250.

DeMaster, D.J., 1981. The supply and accumulation of silica in the marine environment. Geochim. Cosmochim. Acta 45 (10), 1715–1732.

Dubois, N., Kienast, M., Kienast, S., Normandeau, C., Calvert, S.E., Herbert, T.D., Mix, A., 2011. Millennial-scale variations in hydrography and biogeochemistry in the Eastern Equatorial Pacific over the last 100 kyr. Quat. Sci. Rev. 30 (1), 210–223.

Dubois, N., Kienast, M., Kienast, S.S., Timmermann, A., 2014. Millennial-scale atlantic/east pacific sea surface temperature linkages during the last 100,000 years. Earth Planet. Sci. Lett. 396, 134–142.

Dubois, N., Mitchell, N.C., 2012. Large-scale sediment redistribution on the equatorial Pacific seafloor. Deep-Sea Res. I Oceanogr. Res. Pap. 69, 51–61.

Flemming, B.W., 2007. The influence of grain-size analysis methods and sediment mixing on curve shapes and textural parameters: implications for sediment trend analysis. Sediment. Geol. 202 (3), 425–435.

Folk, R.L., Ward, W.C., 1957. Brazos river bar: a study in the significance of grain size parameters. J. Sediment. Res. 27 (1).

Rutgers van der Loeff, M. M., Francois, R., Frank, M., Bacon, M.P., 2004. ^{230}Th normalization: an essential tool for interpreting sedimentary fluxes during the late Quaternary. Paleoceanography 19 (1).

Rutgers van der Loeff, M., Francois, R., Frank, M., Bacon, M.P., Geibert, W., Kienast, S., Anderson, R.F., Bradtmiller, L., Chase, Z., Henderson, G., et al. 2007. Comment on: "Do geochemical estimates of sediment focusing pass the sediment test in the equatorial Pacific?" by M. Lyle et al. Paleoceanography 22 (1).

Gardner, W.D., Sullivan, L.G., Thorndike, E.M., 1984. Long-term photographic, current, and nephelometer observations of manganese nodule environments in the Pacific. Earth Planet. Sci. Lett. 70 (1), 95–109.

Hayes, C.T., Anderson, R., Fleisher, M., 2011. Opal accumulation rates in the Equatorial Pacific and mechanisms of deglaciation. Paleoceanography 26 (1).

Hayes, C.T., Anderson, R.F., Fleisher, M.Q., Huang, K.-F., Robinson, L.F., Lu, Y., Cheng, H., Edwards, R.L., Moran, S.B., 2015. 230 th and 231 pa on GEOTRACES GA03, the US GEOTRACES north Atlantic transect, and implications for modern and paleoceanographic chemical fluxes. Deep-Sea Res. II Top. Stud. Oceanogr. 116, 29–41.

Hayes, C.T., Anderson, R.F., Jaccard, S.L., François, R., Fleisher, M.Q., Soon, M., Gersonde, R., 2013. A new perspective on boundary scavenging in the North Pacific Ocean. Earth Planet. Sci. Lett. 369, 86–97.

Heath, G.R., Moore, T.C., Jr, Roberts, G.L., 1974. Mineralogy of surface sediments from the Panama Basin, eastern equatorial Pacific. The Journal of Geology 145–160.

Henderson, G.M., Anderson, R.F., 2003. The U-series toolbox for paleoceanography. Rev. Mineral. Geochem. 52 (1), 493–531.

Higgins, S.M., Anderson, R.F., Marcantonio, F., Schlosser, P., Stute, M., 2002. Sediment focusing creates 100-ka cycles in interplanetary dust accumulation on the Ontong Java Plateau. Earth Planet. Sci. Lett. 203 (1), 383–397.

Honjo, S., Spencer, D.W., Gardner, W.D., 1992. A sediment trap intercomparison experiment in the Panama Basin, 1979. Deep Sea Res. Part A 39 (2), 333–358.

Johnson, D.A., Johnson, T.C., 1970. Sediment redistribution by bottom currents in the central Pacific. Deep Sea Research and Oceanographic Abstracts. vol. 17. Elsevier., pp. 157–169.

Kienast, M., Kienast, S.S., Calvert, S.E., Eglinton, T.I., Mollenhauer, G., François, R., Mix, A.C., 2006. Eastern Pacific cooling and Atlantic overturning circulation during the last deglaciation. Nature 443 (7113), 846–849.

Kienast, S., Kienast, M., Mix, A.C., Calvert, S., François, R., 2007. Thorium-230 normalized particle flux and sediment focusing in the Panama Basin region during the last 30,000 years. Paleoceanography 22 (2).

Kranck, K., 1975. Sediment deposition from flocculated suspensions. Sedimentology 22 (1), 111–123.

Kranck, K., Milligan, T., 1985. Origin of grain size spectra of suspension deposited sediment. Geo-Mar. Lett. 5 (1), 61–66.

Kranck, K., Smith, P., Milligan, T., 1996a. Grain-size characteristics of fine-grained unflocculated sediments II: "multi-round" distributions. Sedimentology 43 (3), 597–606.

Kranck, K., Smith, P., Milligan, T., 1996b. Grain-size characteristics of fine-grained unflocculated sediments I: "one-round" distributions. Sedimentology 43 (3), 589–594.

Kretschmer, S., Geibert, W., van der Loeff, M.M.R., Mollenhauer, G., 2010. Grain size effects on $^{230}Th_{xs}$ inventories in opal-rich and carbonate-rich marine sediments. Earth Planet. Sci. Lett. 294 (1), 131–142.

Kretschmer, S., Geibert, W., van der Loeff, M.M.R., Schnabel, C., Xu, S., Mollenhauer, G., 2011. Fractionation of ^{230}Th, ^{231}Pa, and ^{10}Be induced by particle size and composition within an opal-rich sediment of the Atlantic Southern Ocean. Geochim. Cosmochim. Acta 75 (22), 6971–6987.

Kusch, S., Eglinton, T.I., Mix, A.C., Mollenhauer, G., 2010. Timescales of lateral sediment transport in the Panama Basin as revealed by radiocarbon ages of alkenones, total organic carbon and foraminifera. Earth Planet. Sci. Lett. 290 (3), 340–350.

Law, B.A., Hill, P., Milligan, T., Curran, K., Wiberg, P., Wheatcroft, R., 2008. Size sorting of fine-grained sediments during erosion: results from the western Gulf of Lions. Cont. Shelf Res. 28 (15), 1935–1946.

Lea, D.W., Pak, D.K., Belanger, C.L., Spero, H.J., Hall, M.A., Shackleton, N.J., 2006. Paleoclimate history of Galapagos surface waters over the last 135,000 yr. Quat. Sci. Rev. 25 (11), 1152–1167.

Ledbetter, M.T., 1986. A late Pleistocene time-series of bottom-current speed in the Vema Channel. Palaeogeogr. Palaeoclimatol. Palaeoecol. 53 (1), 97–105.

Lonsdale, P., Malfait, B., 1974. Abyssal dunes of foraminiferal sand on the Carnegie Ridge. Geol. Soc. Am. Bull. 85 (11), 1697–1712.

Loubere, P., 2000. Marine control of biological production in the eastern equatorial Pacific Ocean. Nature 406 (6795), 497–500.

Loubere, P., Mekik, F., Francois, R., Pichat, S., 2004. Export fluxes of calcite in the eastern equatorial Pacific from the Last Glacial Maximum to present. Paleoceanography 19 (2).

Lyle, M., Marcantonio, F., Moore, W.S., Murray, R.W., Huh, C.-A., Finney, B.P., Murray, D.W., Mix, A.C., 2014. Sediment size fractionation and focusing in the equatorial Pacific: effect on ^{230}Th normalization and paleoflux measurements. Paleoceanography 29 (7), 747–763.

Lyle, M., Mitchell, N., Pisias, N., Mix, A., Martinez, J.I., Paytan, A., 2005. Do geochemical estimates of sediment focusing pass the sediment test in the equatorial Pacific? Paleoceanography 20 (1).

Lyle, M., Mix, A., Pisias, N., 2002. Patterns of $CaCO_3$ deposition in the eastern tropical Pacific Ocean for the last 150 kyr: evidence for a southeast Pacific depositional spike during marine isotope stage (MIS) 2. Paleoceanography 17 (2). 3-1.

Lyle, M., Pisias, N., Paytan, A., Martinez, J.I., Mix, A., 2007. Reply to comment by R. Francois et al. on "Do geochemical estimates of sediment focusing pass the sediment test in the equatorial Pacific?": further explorations of ^{230}Th normalization. Paleoceanography 22 (1).

Mahowald, N., Albani, S., Kok, J.F., Engelstaeder, S., Scanza, R., Ward, D.S., Flanner, M.G., 2014. The size distribution of desert dust aerosols and its impact on the earth system. Aeolian Res. 15, 53–71.

Malfait, B.T., Andel, T.H., 1980. A modern oceanic hardground on the Carnegie Ridge in the eastern Equatorial Pacific. Sedimentology 27 (5), 467–496.

Marcantonio, F., Anderson, R.F., Higgins, S., Stute, M., Schlosser, P., Kubik, P., 2001. Sediment focusing in the central equatorial Pacific Ocean. Paleoceanography 16 (3), 260–267.

Marcantonio, F., Lyle, M., Ibrahim, R., 2014. Particle sorting during sediment redistribution processes and the effect on ^{230}Th-normalized mass accumulation rates. Geophys. Res. Lett. 41 (15), 5547–5554.

McCave, I., Hall, I., 2006. Size sorting in marine muds: processes, pitfalls, and prospects for paleoflow-speed proxies. Geochem. Geophys. Geosyst. 7 (10).

McCave, I., Manighetti, B., Robinson, S., 1995. Sortable silt and fine sediment size/composition slicing: parameters for palaeocurrent speed and palaeoceanography. Paleoceanography 10 (3), 593–610.

McGee, D., Marcantonio, F., McManus, J.F., Winckler, G., 2010. The response of excess ^{230}Th and extraterrestrial ^{3}He to sediment redistribution at the Blake Ridge, western North Atlantic. Earth Planet. Sci. Lett. 299 (1), 138–149.

Middleton, G.V., 1976. Hydraulic interpretation of sand size distributions. J. Geol. 405–426.

Milligan, T., Kranck, K., 1991. Electroresistance Particle Size Analyzers. Principles, Methods and Applications of Particle Size Analysis. Cambridge University Press, New York, pp. 109–118.

Mortlock, R.A., Froelich, P.N., 1989. A simple method for the rapid determination of biogenic opal in pelagic marine sediments. Deep Sea Res. Part A 36 (9), 1415–1426.

Murray, R.W., Leinen, M., 1993. Chemical transport to the seafloor of the equatorial Pacific Ocean across a latitudinal transect at 135°W: tracking sedimentary major, trace, and rare earth element fluxes at the Equator and the Intertropical Convergence Zone. Geochim. Cosmochim. Acta 57 (17), 4141–4163.

Murray, R.W., Leinen, M., Knowlton, C.W., 2012. Links between iron input and opal deposition in the Pleistocene equatorial Pacific Ocean. Nat. Geosci. 5 (4), 270–274.

Patarroyo, G.D., Martínez, J.I., 2015. Late Quaternary sea bottom conditions in the southern Panama basin, eastern equatorial Pacific. J. S. Am. Earth Sci. 63, 346–359.

Paytan, A., Kastner, M., Chavez, F., 1996. Glacial to interglacial fluctuations in productivity in the equatorial Pacific as indicated by marine barite. Science 274 (5291), 1355–1357.

Pena, L., Cacho, I., Ferretti, P., Hall, M., 2008. El Niño-Southern Oscillation-like variability during glacial terminations and interlatitudinal teleconnections. Paleoceanography 23 (3).

Pichat, S., Abouchami, W., Galer, S.J., 2014. Lead isotopes in the eastern equatorial pacific record Quaternary migration of the South Westerlies. Earth Planet. Sci. Lett. 388, 293–305.

Pichat, S., Sims, K.W., François, R., McManus, J.F., Brown Leger, S., Albarède, F., 2004. Lower export production during glacial periods in the equatorial pacific derived from (^{231}Pa/^{230}Th)xs, 0 measurements in deep-sea sediments. Paleoceanography 19 (4).

Prospero, J.M., Bonatti, E., 1969. Continental dust in the atmosphere of the Eastern Equatorial Pacific. J. Geophys. Res. 74 (13), 3362–3371.

Rea, D.K., Hovan, S.A., 1995. Grain size distribution and depositional processes of the mineral component of abyssal sediments: lessons from the North Pacific. Paleoceanography 10 (2), 251–258.

Reimi, M.A., Marcantonio, F., 2016. Constraints on the magnitude of the deglacial migration of the ITCZ in the Central Equatorial Pacific Ocean. Earth Planet. Sci. Lett. 453, 1–8.

Robinson, R., Martinez, P., Pena, L., Cacho, I., 2009. Nitrogen isotopic evidence for deglacial changes in nutrient supply in the eastern equatorial Pacific. Paleoceanography 24 (4).

Saukel, C., Lamy, F., Stuut, J.-B.W., Tiedemann, R., Vogt, C., 2011. Distribution and provenance of wind-blown se Pacific surface sediments. Mar. Geol. 280 (1), 130–142.

Siddall, M., Anderson, R.F., Winckler, G., Henderson, G.M., Bradtmiller, L.I., McGee, D., Franzese, A., Stocker, T.F., Müller, S.A., 2008. Modeling the particle flux effect on distribution of ^{230}Th in the equatorial Pacific. Paleoceanography 23 (2).

Singh, A.K., Marcantonio, F., Lyle, M., 2011. Sediment focusing in the Panama Basin, eastern equatorial Pacific Ocean. Earth Planet. Sci. Lett. 309 (1), 33–44.

Singh, A.K., Marcantonio, F., Lyle, M., 2013. Water column ^{230}Th systematics in the eastern equatorial Pacific Ocean and implications for sediment focusing. Earth Planet. Sci. Lett. 362, 294–304.

Smith, W.H., Sandwell, D.T., 1997. Global sea floor topography from satellite altimetry and ship depth soundings. Science 277 (5334), 1956–1962.

Snoeckx, H., Rea, D.K., 1994. Dry bulk density and $CaCO_3$ relationships in upper Quaternary sediments of the eastern equatorial Pacific. Mar. Geol. 120 (34), 327–333.

Suman, D.O., Bacon, M.P., 1989. Variations in Holocene sedimentation in the North American Basin determined from ^{230}Th measurements. Deep Sea Res. Part A 36 (6), 869–878.

Thomson, J., Colley, S., Anderson, R., Cook, G., MacKenzie, A., Harkness, D., 1993. Holocene sediment fluxes in the northeast Atlantic from $^{230}Th_{excess}$ and radiocarbon measurements. Paleoceanography 8 (5), 631–650.

Van Andel, T.H., 1973. Texture and dispersal of sediments in the Panama Basin. J. Geol. 434–457.

Winckler, G., Anderson, R.F., Jaccard, S.L., Marcantonio, F., 2016. Ocean dynamics, not dust, have controlled equatorial pacific productivity over the past 500,000 years. Proc. Natl. Acad. Sci. 113 (22), 6119–6124.